

Supplementary Information:

Dynamics of Phase-Separated Microdroplets Near the Contact Line of Evaporating All-Aqueous Drops

Rahul Rai[†], Maheshwar Gopu[†], Senthana Pugalneelam Parameswaran, Tapan Chandra Adhyapak, and Dileep Mampallil[‡]

[†] Equal contribution

Department of Physics, Indian Institute of Science Education and Research
Tirupati, Yerpedu, Tirupati - 517619, Andhra Pradesh, India.

[‡] E-mail: dileep.mampallil@iisertirupati.ac.in; adhyapak@iisertirupati.ac.in

CONTENTS

1	Experimental details	1
2	COMSOL calculations- Marangoni convective flow	1
3	COMSOL simulation- droplet coalescence	4
4	Supplementary video 1	6
5	Supplementary video 2	6
6	Supplementary figures	7

1. EXPERIMENTAL DETAILS

In the experiments, we allowed the evaporation of a polymer mixture drop of volume $1\ \mu\text{l}$. The completion of the evaporation took about 7 minutes. The initial concentrations of individual polymers (DEX, $M_w = 40000\ \text{g/mol}$ and PEG, $M_w = 6000\ \text{g/mol}$) were prepared at 2 - 10 wt% in deionized water and combined appropriately to prepare the polymer-mixture solutions at the required concentration ratio. When fluorescein isothiocyanate (FITC)-DEX ($M_w = 10000\ \text{g/mol}$, $\lambda_{\text{em}} = 517\ \text{nm}$) was used, its concentration was set to 1 wt% and mixed with the non-fluorescent DEX. All the chemicals were purchased from Sigma Aldrich.

2. COMSOL CALCULATIONS- MARANGONI CONVECTIVE FLOW

We solved incompressible fluid flow governed by the equation of continuity and the Navier-Stokes equations, the diffusion equation to obtain the concentration distribution of vapor in the air, and the heat equation with convective term to obtain the thermal distribution on the liquid-air interface. We considered an axisymmetric sessile water drop of radius $R = 1\ \text{mm}$, initially in thermal equilibrium with the solid substrate at $25\ ^\circ\text{C}$. While the evaporation rates are higher near the edge of the droplet [1, 2], any temperature change in that region is counterbalanced by thermal conduction from the substrate. However, the apex of the droplet has a longer thermal

conduction path to the substrate, leading to a colder temperature compared to the edge. For the simplicity of calculation, we set a constant equilibrium contact angle as $\pi/2$, a value different from the experimental case ($\sim 23 \pm 1^\circ$). Since the contact angle dependence of the Marangoni effect is only weak [3], this difference does not significantly affect the conclusions drawn from the simulation.

We have followed a similar calculation procedure as in the COMSOL Application (ID 97071) on Droplet Evaporation on Solid Surfaces, freely available in the Application Library. The axisymmetric evaporation model was designed by coupling the following components.

- (i) Laminar Flow (LF)
- (ii) Transport of Diluted Species (TDS)
- (iii) Heat Transfer in Solid and Fluids (HT)

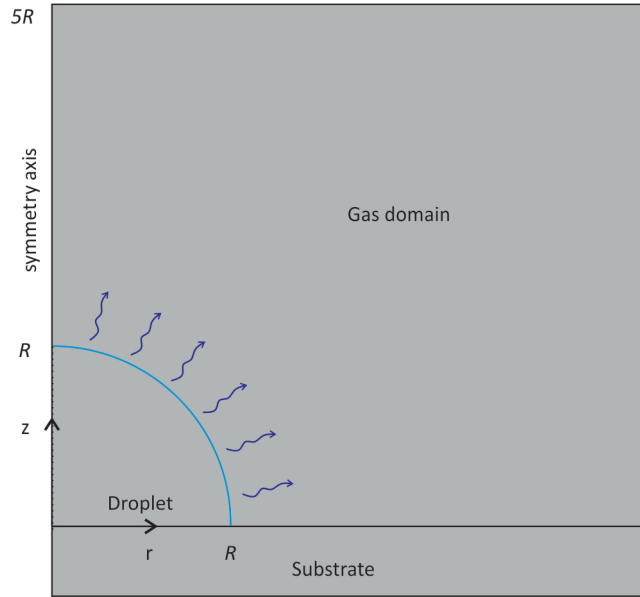


Fig. S1. Illustration of the computational domain. The evaporating part of the drop represented by curvy arrows.

Initial conditions: We kept the initial temperature constant (298.15 K) throughout the computational domain. The fluid velocity was zero. The pressure surrounding the droplet is considered as 1 atm.

The governing equations of the flow are,

$$\frac{\partial \rho}{\partial t} + \nabla \cdot (\rho \vec{u}) = 0, \quad (\text{S1})$$

$$\rho \left(\frac{\partial \vec{u}}{\partial t} + \vec{u} \cdot \nabla \vec{u} \right) = -\nabla p + \mu \nabla \cdot (\nabla \vec{u}), \quad (\text{S2})$$

where ρ is the density, p is the pressure, \vec{u} is the velocity, and μ is the viscosity of water. We neglected the inertial effects.

Boundary conditions:

The inertial terms in Eq.S2 are omitted. We used the Navier slip boundary condition with the minimum element length factor 0.5 at the solid-liquid and solid-air interfaces. For the rest of the bottom, we used a no-slip boundary condition. Far from the drop, the boundary is set as the open boundary with zero normal stress.

At the evaporating Fluid-Fluid Interface, the outward mass flux was set as $J = D(1 - H)c_v/R$. Here, D is the diffusion coefficient, H is the relative humidity, c_v is the saturation vapor concentration, and R is the radius of the drop.

Transport of Dilute Species:

We used the Transport of Diluted Species module in COMSOL to model mass transport from the air-water interface. The governing equation is given by,

$$\frac{\partial c}{\partial t} + \vec{u} \cdot \nabla c = \nabla \cdot (D \nabla c), \quad (\text{S3})$$

where c is the concentration of the species. We initially set the vapor concentration as zero in the air, and the vapor concentration at the water-air interface is set as c_{sat} .

We obtained the temperature distribution in the drop by solving,

$$\rho c_p \vec{u} \cdot \nabla T - \nabla \cdot (k \nabla T) = -\rho c_p \frac{\partial T}{\partial t} \quad (\text{S4})$$

where T is the temperature, k is the thermal conductivity, and ρ and c_p are the density and specific heat capacity of the fluid, respectively. The boundary conditions used to solve Eq. (S4) are given as,

$$T = 298.15 \text{ K} \quad \text{for a boundary far from the drop,} \quad (\text{S5})$$

$$\Delta H = -J L_w \quad \text{at the evaporating interface,} \quad (\text{S6})$$

$$T_w = T_a \quad \text{at the air (a)-water (w) interface,} \quad (\text{S7})$$

$$T_w = T_s, \quad -k_w \nabla T_w = -k_s \nabla T_s \quad \text{at the water (w)-solid (s) interface,} \quad (\text{S8})$$

where L_w is the latent heat of vaporization, and the subscripts w , a , and s denote water, air, and solid, respectively. The cooling effect of evaporation (ΔH) was used as the boundary heat source at the evaporating fluid-fluid interface.

To calculate the Marangoni flow, we have incorporated an additional Laminar Flow (LF2) component and Marangoni Effect component in the Multiphysics. The temperature distribution simulated using the Heat Transfer interface was used as the input to calculate the Marangoni stress across the fluid-air interface. The thermal Marangoni stress at the fluid-air interface is given by τ_m ,

$$\vec{\tau}_m = \frac{d\sigma}{dT} \nabla T, \quad (\text{S9})$$

at $z = h(r, t)$ and $z > 0$, where $d\sigma/dT$ is the surface tension gradient with respect to temperature. We used no-slip boundary conditions at the solid wall. We took the value of $d\sigma/dT$ as $-0.165 \times 10^{-3} \text{ N/mK}$.

Furthermore, the details on boundary conditions and calculations can be found in the application model or ref. [4-6].

3. COMSOL SIMULATION- DROPLET COALESCENCE

To obtain the exact variation of ϕ during the coalescence, we have performed numerical simulations using COMSOL multiphysics. In short, we considered two 2D drops of radius $20\ \mu\text{m}$ placed in a viscous fluid. The viscosity of the inner and outer fluid was set as $10\ \text{mPa}\cdot\text{s}$. The interfacial tension between the drop and the surrounding liquid was set as $10\ \mu\text{N}/\text{m}$. The interfacial energy minimization and the flow were solved simultaneously using the Phase Field and Laminar Flow modules in COMSOL.

Fig.S2 illustrates the shape changes during coalescence. ϕ peaks when the ellipsoid's major axis aligns with \hat{l} . As a result of coalescence, the ϕ value for a single drop (marked with a star bullet in Fig.S2) peaks and then decreases to the value of the combined droplet. This indicates a peak behavior in the Marangoni driving force and the corresponding velocity u_M during coalescence.

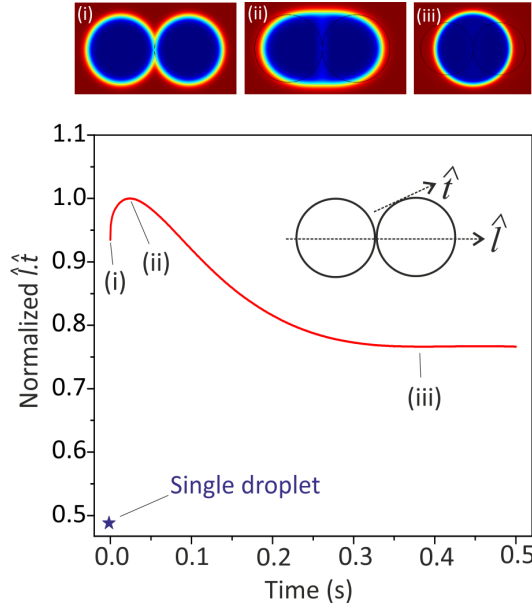


Fig. S2. Shape change during the coalescence of two drops (numerical calculation). Graph shows normalized $|\hat{l} \cdot \hat{t}|$ during the coalescence. The numbering shows time points of shapes. The value of normalized $|\hat{l} \cdot \hat{t}|$ for a single drop is also marked with a star bullet.

REFERENCES

1. R. D. Deegan, O. Bakajin, T. F. Dupont, G. Huber, S. R. Nagel, and T. A. Witten, "Contact line deposits in an evaporating drop," *Phys. review E* **62**, 756–765 (2000).
2. H. Hu and R. G. Larson, "Marangoni effect reverses coffee-ring depositions," *The J. Phys. Chem. B* **110**, 7090–7094 (2006).
3. L. Wang, Z. Liu, X. Wang, and Y. Yan, "Investigation on the droplet evaporation process on local heated substrates with different wettability," *Heat Mass Transf.* pp. 1–13 (2020).
4. B. Bozorgmehr and B. T. Murray, "Numerical simulation of evaporation of ethanol–water mixture droplets on isothermal and heated substrates," *ACS Omega* **6**, 12577–12590 (2021).
5. R. van Gaalen, H. Wijshoff, J. Kuerten, and C. Diddens, "Competition between thermal and

- surfactant-induced marangoni flow in evaporating sessile droplets,” *J. Colloid Interface Sci.* **622**, 892–903 (2022).
6. M. R. Barmi and C. D. Meinhart, “Convective flows in evaporating sessile droplets,” *The J. Phys. Chem. B* **118**, 2414–2421 (2014).
 7. J. C. Crocker and D. G. Grier, “Methods of Digital Video Microscopy for Colloidal Studies,” *J. Colloid Interface Sci.* **179**, 298–310 (1996).

4. SUPPLEMENTARY VIDEO 1

Evaporation of 1 μL PEG-DEX drop on a cleaned glass surface, the video was captured close to the contact line. As the drop evaporates, the DEX nucleations coalesce with nearby microdroplets and perform step-wise motion towards the center of the drop. The video was recorded at 24 fps. The initial concentration of PEG-DEX in the drop was 2 wt%, 10 wt%, respectively.

5. SUPPLEMENTARY VIDEO 2

Evaporation of 1 μL PEG-DEX drop on a cleaned glass surface, the video was captured close to the contact line. Tracking of the droplet was done using a custom Matlab algorithm [7]. The velocity vs time plot below has a corresponding peak for every coalescence event. The video was recorded at 200 fps and playing at 50 fps. The initial concentration of PEG-DEX in the drop was 2 wt%, 10 wt%, respectively.

6. SUPPLEMENTARY FIGURES

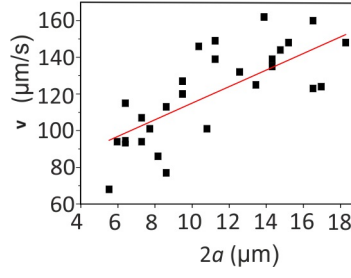


Fig. S3.

Migration velocity and droplet diameter: The average velocity of continuously moving droplets (in *region B*) as a function of their diameter shows a linear relationship as expected ($v \propto a$). The microdroplets reach *region B* after a cascade of coalescence events. In this region, they move continuously as they are large. Since the their velocity increases as they move, we plotted their average velocity.

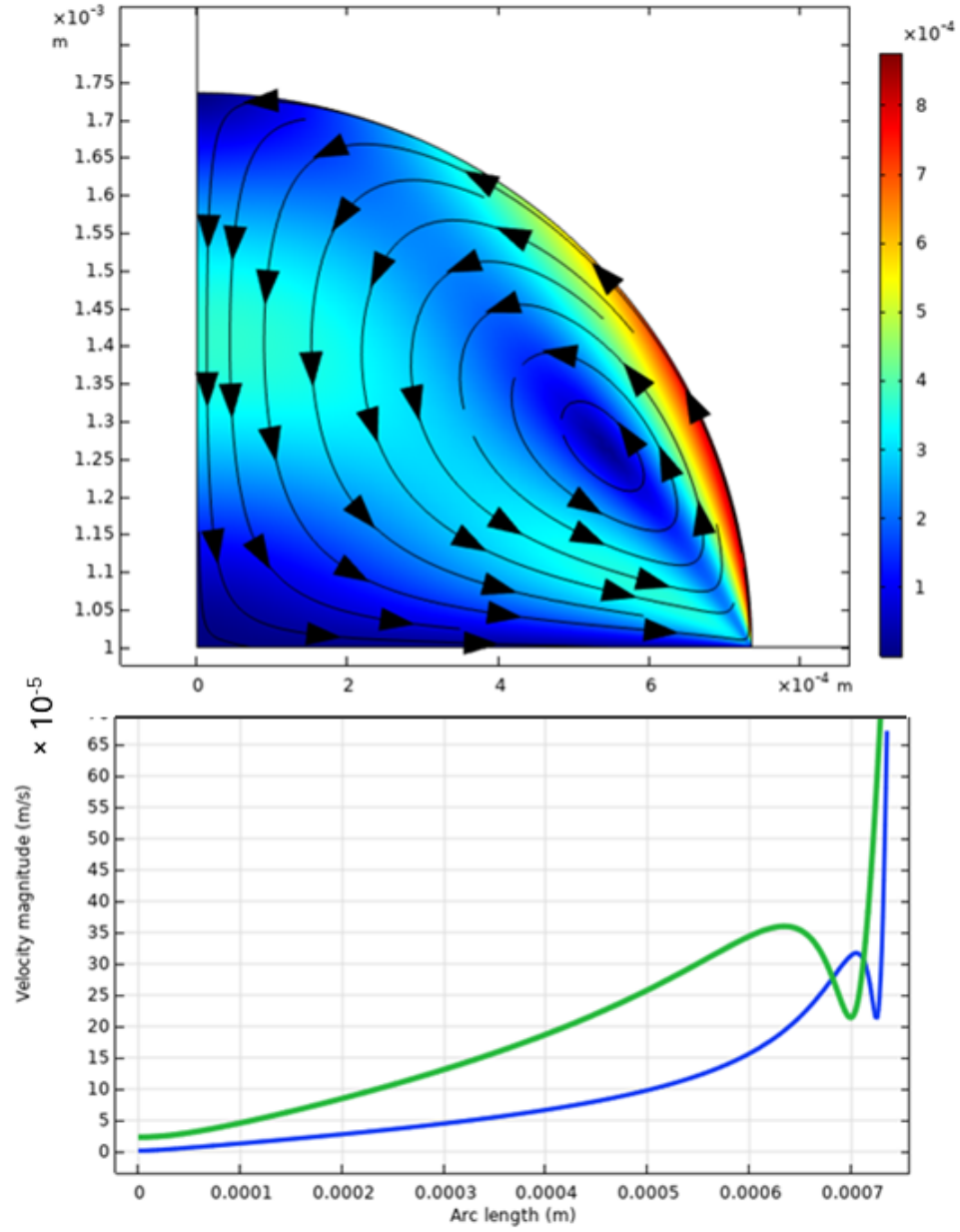


Fig. S4. Flow patterns at large surface tension gradient: The flow pattern is circulating, and thus, the flow strength gradient exists even at very large interfacial stresses at the liquid-air interface. In this case, a large interfacial stress (ten times that in Fig.2 in the main article) was applied in the simulation manually. The green and blue curves correspond cutline at two heights: 3 and 10 micrometers.

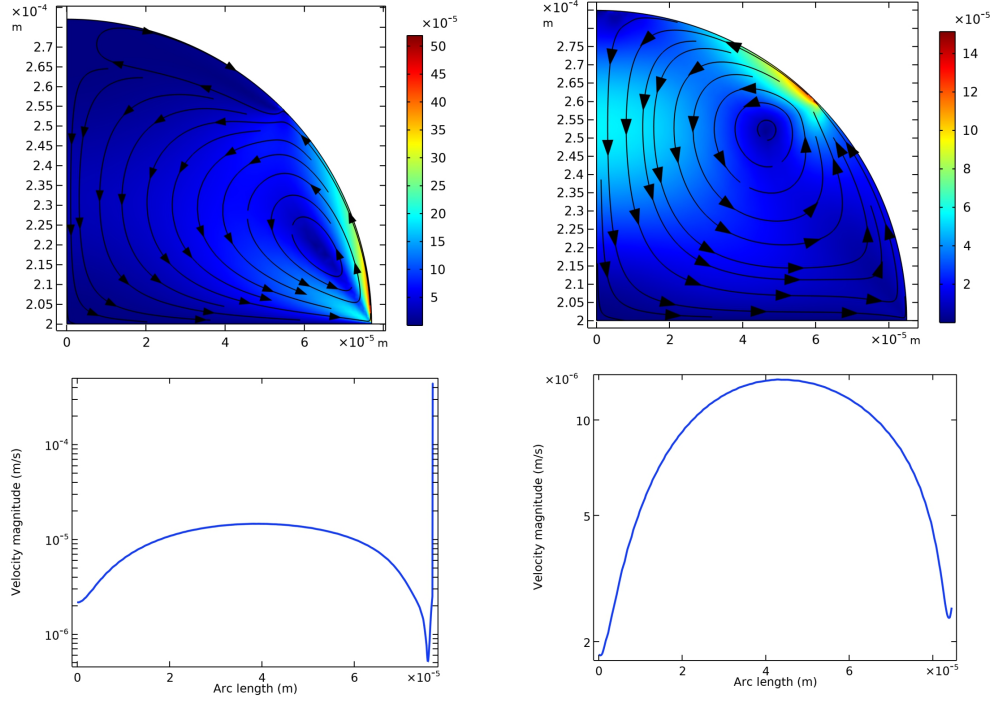


Fig. S5. Position of the flow pattern: The variation of the strength of the flow near the substrate depends on the position of the flow pattern. In the COMSOL calculations, the positions were manipulated by setting only a certain region of the drop is evaporating. (Left): The lower region swept by an angle $\pi/4$ from the horizontal is evaporating and the other upper $\pi/4$ segment is set as non evaporating. This theoretical construct created the flow pattern close to the substrate. (Right): When the upper segment was evaporating the flow patterns were located away from the substrate. Both the scenarios resulted in different spatial rate of change of the flow strength corresponding to a horizontal cutline $3 \mu\text{m}$ above the substrate. These results show that the variation of the flow strength near the contact line depends upon the position of the flow circulation.

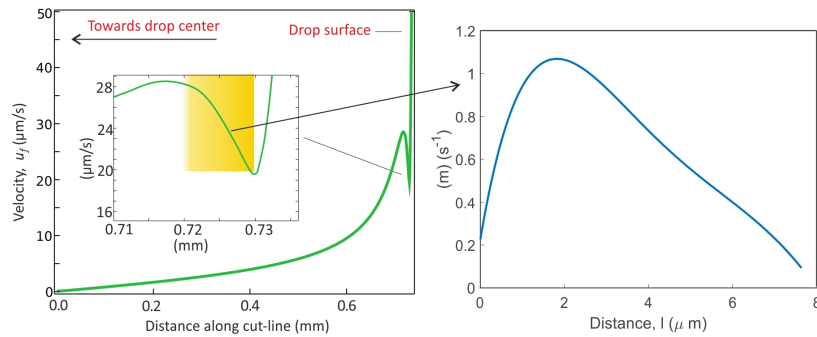


Fig. S6. Gradient of flow strength m from the COMSOL data: The droplets moving radially inward experience increasing flow strength in the region highlighted in the flow profile near the substrate (left panel). The slope of the velocity curve in this region small near the contact line and far away (right panel). Thus, during a cascade of coalescence events and migration of the microdroplets, the gradient strength (slope of the velocity curve) of the background flow experienced by the droplets varies. It has a consequence in the step length $\Delta\ell$ and average (or peak) velocity of the microdroplet during a coalescence event. See also Fig.4(d) in the main manuscript.

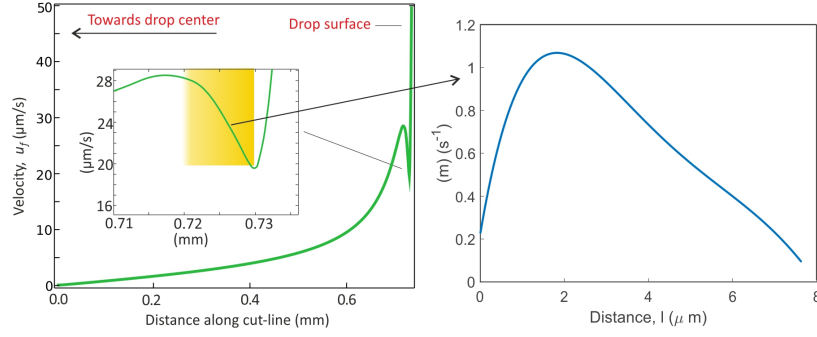


Fig. S7. Gradient of flow strength m from the COMSOL data: The droplets moving radially inward experience increasing flow strength in the region highlighted in the flow profile near the substrate (left panel). The slope of the velocity curve in this region small near the contact line and far away (right panel). Thus, during a cascade of coalescence events and migration of the microdroplets, the gradient strength (slope of the velocity curve) of the background flow experienced by the droplets varies. It has a consequence in the step length Δl and average (or peak) velocity of the microdroplet during a coalescence event. See also Fig.4(d) in the main manuscript.

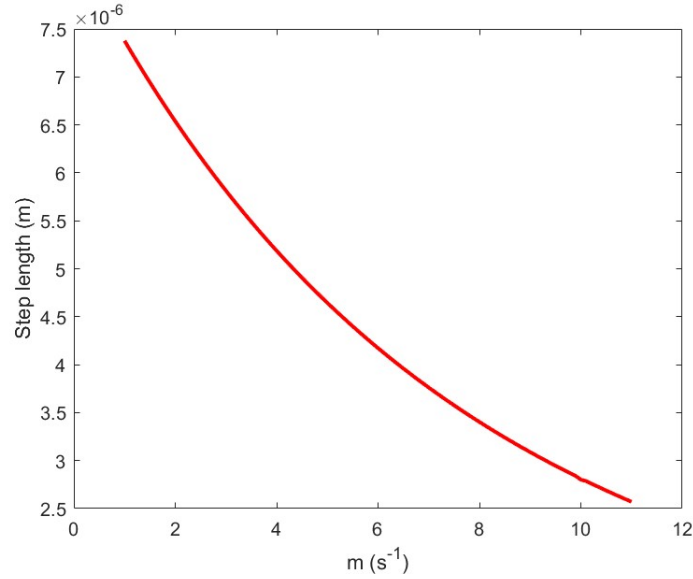


Fig. S8. Analytical model- Step length (Δl) versus flow gradient strength With increasing m , the step length decreases. Also see Fig.4(d) in the main manuscript.

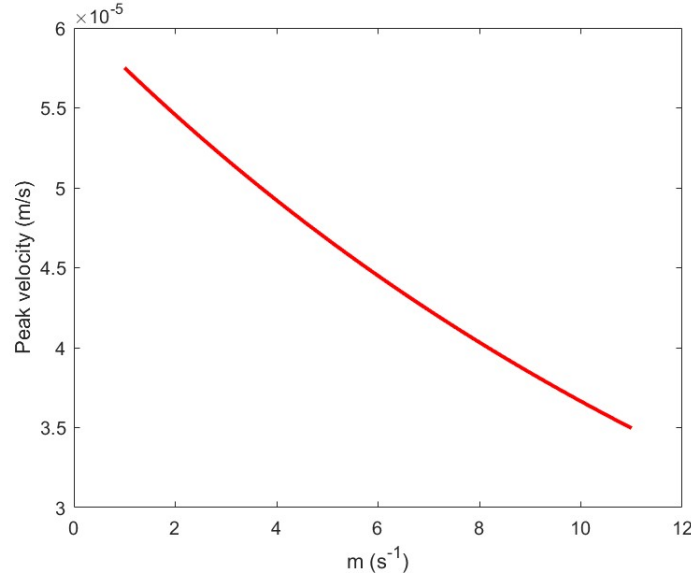


Fig. S9. Analytical model-Peak velocity versus flow gradient strength: The peak value of the velocity depends upon the strength of the background flow gradient (m). With increasing m , the value of v_{peak} decreases.

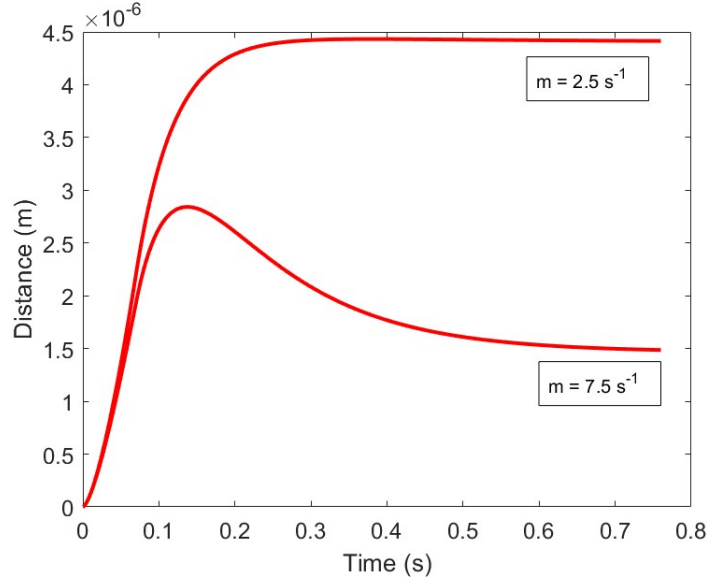


Fig. S10. Velocity reversal at large m : When the background flow strength gradient (m) is large, in each coalescent-induced steps, the forward velocity of the DEX nuclei can match with that of the background flow before the completion of the shape relaxation. However, the shape relaxation continuous and it decreases the Marangoni force as the ellipsoidal shape becomes sphere. As a consequence of decreased forward flow velocity (v_M), we can anticipate that the nuclei can partially move backward to a new equilibrium position. This aspect can be seen in the plot corresponding to $m = 7.5 \text{ s}^{-1}$, where the curve decreases after peaking. In this decreasing region, we observe a negative velocity. Observing this slight reverse movement of the microdroplets is challenging experimentally, at least in our system, probably due to small m values. ($a = 5 \text{ }\mu\text{m}$, $b_0 = 40 \text{ s}^{-3/2}$, $b = 8 \times 10^{-4}$, and $\tau_{vc} = 0.05$.)